

# Mind the Gap: Standard 3DGS Evaluation Primarily Measures Near-Trajectory Interpolation

Gaoxiang Jia\* Vikram Appia

Advanced Micro Devices, Inc.

\*Corresponding author: jiagaoxiang@gmail.com

## Abstract

Standard MipNeRF360-style 3D Gaussian Splatting (3DGS) evaluation holds out every  $N$ -th frame—but these frames have trained neighbors on both sides, so the metric measures *near-trajectory interpolation* rather than spatial generalization. We introduce a *fair matched-count* protocol that isolates this effect: both arms train on the same number of images and differ only in whether the holdout is spread evenly (interpolation) or forms a contiguous spatial sector (extrapolation). Our primary finding is a large, consistent interpolation–extrapolation gap of **3–12 dB**—several times the differences typically reported between competing methods. The gap is robust to training noise, is in two cases large enough to flip a method ranking under multi-seed confirmation, and—crucially—persists across three representation families, including a non-Gaussian volumetric neural radiance field (NeRF), so it reflects spatial coverage rather than any one representation. Diagnostically, it is dominated by a diffuse/geometry-proxy component and tracks each view’s angular distance to its nearest training view, a zero-cost signal that also guides capture planning; loss-side regularization yields only marginal gains. Standard holdouts remain useful for near-trajectory rendering but should not, alone, be read as evidence of spatial generalization. Prior work notes protocol sensitivity; ours is, to our knowledge, the first to combine matched-count paired holdout, cross-representation quantification, and a diagnostic analysis (Table 1). We describe a *spatial-holdout benchmark toolkit* with standardized splits and baselines for 16 scenes, which we are preparing for public release.

## 1 Introduction

3D Gaussian Splatting (3DGS) [1] has rapidly become the preferred representation for real-time novel-view synthesis [17], owing to its explicit scene representation and efficient rasterization. Building on this foundation, recent *world-model* pipelines generate panoramic environments and then reconstruct them as 3DGS scenes using video-diffusion models to produce multi-view training frames [2, 3, 4].

A critical question underlies all such systems: *how do we know the 3D reconstruction is any good?* The standard

answer is peak signal-to-noise ratio (PSNR), structural similarity (SSIM), and learned perceptual image patch similarity (LPIPS) computed on held-out views selected by subsampling every  $N$ -th frame from an ordered camera sequence. This `test_every` convention, used since the original 3DGS [1], has a structural limitation: each held-out frame has trained neighbors on both sides, so the metric primarily measures how well the model *interpolates* between nearby trained views rather than how well it generalizes to unseen spatial regions.

**Why extrapolation matters.** Many applications require *spatial generalization*, not just near-trajectory rendering: driving simulators render adjacent-lane views [21, 22], virtual and augmented reality (VR/AR) lets users move beyond the captured path, sparse-capture (real estate, e-commerce) synthesizes from few photos, and world-model pipelines generate training data from novel viewpoints [2, 3]. Yet even for near-capture rendering the standard metric gives *false confidence*: a model scoring 30+ dB on interpolation can drop to 18–25 dB on spatial holdout (Table 3), with no warning. A benchmark that claims “novel-view synthesis” but tests near-neighbor interpolation can inadvertently steer method selection toward reproducing training views rather than generalizing.

Prior work has observed aspects of this problem [18, 21, 22, 10, 42, 43]. However, no existing study combines these axes (Table 1): (1) matched training-set size, (2) a dB gap across multiple methods and scenes, (3) multi-seed-confirmed ranking changes under that protocol, (4) a spherical harmonic (SH) degree analysis, and (5) generality across representation families—feed-forward Gaussians *and* a non-Gaussian volumetric NeRF. In short: prior work observes protocol sensitivity; we provide the first matched-count, multi-representation benchmark with a diagnostic analysis, showing the effect is *larger than method deltas*.

We propose a **fair matched-count comparison**: hold out the same number of images either spread evenly (interpolation, the standard protocol) or as a contiguous angular sector (extrapolation). Both arms train on identical data counts and evaluate on genuinely unseen images—the designed contrast is the spatial distribution of the holdout. Across 16 scenes (10 real-capture, 6 generated-view) and

three published 3DGS implementations, we consistently measure gaps of **3–12 dB**—larger than the performance differences typically reported between published methods (Table 3: inter-method range  $<2.5$  dB on interpolation). A method comparison claiming “0.5 dB better” is making a claim smaller than the gap between evaluation modes.

Our contributions:

1. A **fair matched-count evaluation protocol** that measures interpolation and extrapolation on genuinely unseen images with identical training data counts (§3).
2. A **systematic quantification** of the gap across 16 scenes, 3 methods, and 502 training runs with targeted multi-seed validation—showing the gap is  $39\times$  larger than training noise and is, in two multi-seed-confirmed cases, consequential for method ranking (§4).
3. **Mechanistic decomposition**: SH-degree analysis attributes 62% of the gap to a diffuse/geometry-proxy component and 38% to view-dependent color, with higher SH degrees *hurting* extrapolation on 3/9 scenes (§5). Per-image quality correlates with nearest-training-view distance ( $r = -0.58$ ,  $n = 492$ ), providing a zero-cost diagnostic.
4. **Coverage-guided view selection**: a zero-cost heuristic that outperforms random placement on 31/40 scene-budget combinations (10 scenes, 240 runs), strongest at  $M = 1$  (9/10 scenes).
5. **Cross-representation generality**: under our matched-count protocol the gap persists in a non-Gaussian NeRF (Instant-NGP;  $+3.7$  dB,  $r = 0.90$  with the 3DGS gap), and an analogous gap appears in two feed-forward methods under a distance-based target protocol (MVSplat, DepthSplat;  $+7$ – $9$  dB in-domain on RealEstate10K)—the effect tracks spatial coverage, not Gaussian primitives (§5, §7).
6. A **spatial-holdout benchmark toolkit**: split generation, a one-command evaluator, and a pose-only coverage diagnostic, with standardized splits and baseline metrics for 16 scenes (Appendix E).<sup>1</sup>

## 2 Related Work

**3D Gaussian Splatting.** 3DGS [1] represents scenes as collections of anisotropic 3D Gaussians with learned positions, covariances, opacities, and spherical harmonic coefficients. Subsequent work has improved densification [11, 30], introduced structured anchors [31], pursued compression [13, 32], anti-aliasing [12], 2D formulations [14],

<sup>1</sup>The benchmark toolkit and accompanying code are still in preparation for release; we plan to make them publicly available in a future revision of this paper. In the meantime, the protocol, split-construction rule, and per-scene configurations are documented in full in the appendix so the results can be reproduced independently.

progressive propagation [33], principled pruning [40], efficient densification [20], and appearance embedding [8, 19]. Feed-forward methods predict Gaussians directly from sparse images [35, 36, 34, 38], bypassing per-scene optimization but inheriting training-distribution coverage assumptions. Nearly all of these report results under the standard Mip-NeRF360 protocol, commonly using every 8th ordered image as a test view; our experiments show that this sequential-holdout setting can be systematically biased when the ordered images lie on smooth camera trajectories.

**Generated-View 3DGS.** World-model pipelines generate multi-view training data from panoramic images using video-diffusion models [2, 3, 4, 5]. Related systems include LucidDreamer [15], ZeroNVS [16], and WildGaussians [41] for in-the-wild captures. These systems use a mix of evaluation protocols, including held-out target views, fixed render paths, and within-trajectory splits. Our critique applies specifically when evaluation holds out frames along the same smooth generated trajectory: the held-out frames are then interpolation on the generated path rather than spatial extrapolation.

**Evaluation of Novel-View Synthesis.** A growing body of work identifies limitations in standard novel-view synthesis (NVS) evaluation. Several propose separate train/test trajectories or extrapolation benchmarks [18, 21, 22, 44, 45, 23, 27, 28], and others show evaluation protocol can change or even invert reported rankings [10, 43, 26]. Closest to us, FreeVS [42] independently observes that periodic frame holdout is “novel frame synthesis” rather than novel-view synthesis and proposes dropping camera viewpoints—a convergent diagnosis that underscores the problem’s importance. Our work differs in three ways that, to our knowledge, no prior study combines (Table 1): a *matched-count* protocol (both arms train on  $N - K$  images, removing the data-count confound that makes prior comparisons ambiguous); a *quantified* dB gap across methods, scenes, and representation families; and a *diagnostic* analysis (SH decomposition, angular-distance correlation) rather than an observation alone.

**Regularization for 3DGS Generalization.** RegNeRF [46] pioneered regularization from unseen viewpoints for few-shot NeRF; several 3DGS works build on this principle. ICO-GS [24] identifies “appearance compensation”—the optimizer adjusting color/opacity to mask geometric errors—as a key failure mode under sparse views. DropoutGS [25] and the concurrent DropGaussian [47] independently propose randomly dropping Gaussians during training for sparse-view robustness. CoherentGS [29] addresses sparse-view overfitting by seeking flatter loss landscapes, while FASR [48] extends

Table 1: **Comparison with prior evaluation studies** along axes we combine; entries reflect each work’s *primary reported protocol*, not a judgment of quality. *Matched count*: interp and extrap arms train on the same number of images. *Paired interp/ext*: both modes measured on the same scenes under one protocol. *Multi-method*:  $\geq 2$  reconstruction methods compared. To our knowledge ours is the first to combine all listed axes.

	<i>Matched count</i>	<i>Paired interp/ext</i>	<i>Multi-method</i>	<i>Real-generated</i>	<i>Multi-seed</i>	<i>SH analysis</i>	<i>Toolkit</i>
Nerfbusters [18]							
NeRF Dir. [43]		✓					
EUVS [21]			✓				
VEGS [22]							
FreeVS [42]			✓				
NerfBase. [10]			✓				✓
<b>Ours</b>	✓	✓	✓	✓	✓	✓	✓

this with frequency-adaptive sharpness-aware minimization. Co-Adaptation [49] formalizes why Gaussians become entangled to fit training views and provides theoretical justification for dropout-based regularization. DN-Splatter [39] incorporates depth and normal priors for improved geometry. Our work extends these insights to the evaluation-gap setting: we test Gaussian dropout as a view-specialization regularizer and find its effect is scene-dependent—it does not universally reduce the gap, suggesting that the gap is largely a data-coverage problem.

### 3 Method

#### 3.1 Problem Statement

The standard 3DGS evaluation protocol [1] sorts images by filename, holds out every 8th image as the test set, and trains on the remaining  $\sim 87.5\%$ . Each held-out image has trained neighbors on both sides—the metric measures how well the model *interpolates* between nearby views, not how well it synthesizes genuinely novel viewpoints from unseen spatial regions.

#### 3.2 Fair Matched-Count Protocol

We propose a controlled comparison (Figure 1) that isolates the effect of holdout spatial distribution while eliminating data-count confounds. Given a scene with  $N$  cameras:

- Interpolation arm (standard protocol).** Hold out every 8th image by sorted filename ( $K = \lceil N/8 \rceil$  images). Train on  $N - K$  images. Evaluate on the  $K$  held-out images. Each held-out image has trained neighbors on both sides—this measures *interpolation*.

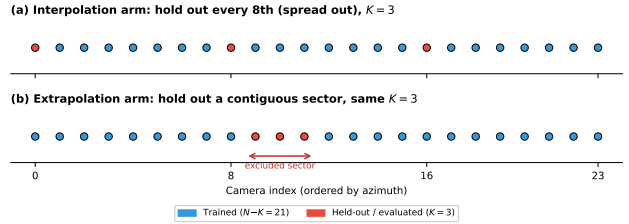


Figure 1: **Interpolation vs. extrapolation evaluation.**

(a) Standard evaluation: held-out frames (red) have trained neighbors on both sides—the metric measures interpolation. (b) Spatial-holdout evaluation: a contiguous region is excluded from training. Held-out frames now have no nearby training views—the metric measures extrapolation. Our fair matched-count protocol ensures both arms train on the same number of images and evaluate on the same number of held-out images (though the specific images differ).

- Extrapolation arm (sector holdout).** Sort cameras by azimuth around the scene centroid. Starting from a random position (seed 42), hold out  $K$  *contiguous* cameras. Train on  $N - K$  images. Evaluate on  $K$  held-out images (different images than the interp arm, but the same count). Test views have substantially larger nearest-training-view distances—this measures *extrapolation*.

The gap is defined as:

$$\Delta = \text{PSNR}_{\text{interp}} - \text{PSNR}_{\text{extrap}} \quad (1)$$

Both arms train on exactly  $N - K$  images and evaluate on exactly  $K$  genuinely unseen images. The designed contrast is whether the held-out images are spatially interleaved with training views (interpolation) or concentrated in an unseen region (extrapolation). By fixing the same held-out count  $K$  for both arms, the comparison isolates the effect of the hold-out’s spatial distribution rather than the amount of training data.

## 4 The Interpolation–Extrapolation Gap

### 4.1 Experimental Setup

We evaluate the gap on two data regimes:

**Real-capture scenes.** Nine scenes from MipNeRF360 [6] (5 outdoor: bicycle, flowers, garden, stump, treehill; 4 indoor: bonsai, counter, kitchen, room) and one from Tanks and Temples [7] (truck). Outdoor scenes use `images_4` (quarter resolution); indoor scenes use `images_2` (half resolution), following standard practice.

**Generated-view scenes.** Six scenes from the HY-World 2.0 [2] panorama-to-3D pipeline: two from the re-

leased demo examples (case000, a garden patio: 199 images; case001, a living room: 178 images) and four generated by us from CC0 equirectangular panoramas (courtyard, gazebo, yaris, alps: 283 images each). All were converted to COLMAP format for cross-method comparison.

**Methods.** Three published 3DGS implementations, each with default hyperparameters and 30K training iterations: Official 3DGS [1] (with gsplat [9]), Mip-Splatting [12] (`kernel_size` = 0.1), and 3DGS Markov chain Monte Carlo (3DGS-MCMC) [30]. To test representation-independence (§5.3) we additionally train a non-Gaussian volumetric NeRF, Instant-NGP [56] (hash-grid encoding, nerface [57] occupancy-grid rendering, 20K steps), under the same per-arm split files. Total: 502 training runs including multi-seed validation, multi-sector robustness, and regularizer ablations.

## 4.2 Main Results

**Real captures.** Table 3 shows the gap across 10 real-capture scenes. *Every scene and every method* shows a positive gap, ranging from **3.2 to 11.1 dB** (mean 5.84 dB for Official 3DGS). The gap is consistent across all three metrics: SSIM shows a mean gap of 0.124 and LPIPS of 0.086 (Appendix A). It is consistently larger than the inter-method performance differences on the same scenes (<2.5 dB on standard benchmarks).

**Generated views.** Table 2 shows the gap on 6 generated-view scenes. The gap ranges from **3.3 to 12.0 dB** (mean 8.4 dB)—about **1.4×** the real-capture gap. The two HY-World example scenes (case000, case001) show the largest gaps (10–12 dB), while the four scenes generated from CC0 panoramas show gaps of 3.3–10.2 dB. Mip-Splatting vs. Official 3DGS shows 2/6 ranking reversals (case001, gazebo). This suggests that video-diffusion-generated data is susceptible to the same evaluation pattern as real captures, likely because generated trajectories follow smooth paths.

**Ranking reversals.** Multi-seed validation on both methods confirms two *robust* reversals (★ in Table 3): **garden** (Mip wins interp +0.07, Official wins extrap +0.52; 93% of pairwise seed combos) and **bicycle** (Mip wins interp +0.15, Official wins extrap +0.22; 89%). Other scenes do not show robust reversals under multi-seed. The consistent gap *direction* (interp > extrap) across all 48 scene-method combinations is the primary finding; the two robust reversals demonstrate that the gap can be practically consequential for method selection.

**The gap is not just harder images.** A natural objection is that extrapolation views are simply intrinsically harder.

Table 2: **Generated-view gap** (6 HY-World scenes, fair matched-count protocol). Gaps are  $\sim 1.4\times$  real-capture gaps. Numbers in parentheses are the per-column method rank (1=best). †Ranking reversal: the Mip-Splatting vs. Official order flips between interp and extrap (single-run; not multi-seed confirmed).

Scene	Method	Interp	Extrap	Gap
case000	Official 3DGS	31.36 (3)	19.40 (3)	11.96
	Mip-Splatting	31.68 (2)	19.67 (2)	12.01
	3DGS-MCMC	<b>31.82</b> (1)	<b>19.85</b> (1)	11.97
case001†	Official 3DGS	24.34 (3)	14.63 (2)	9.71
	Mip-Splatting	24.52 (2)	14.44 (3)	10.08
	3DGS-MCMC	<b>25.67</b> (1)	<b>14.67</b> (1)	11.00
courtyard	Official 3DGS	21.83 (3)	14.40 (3)	7.43
	Mip-Splatting	22.00 (2)	14.62 (2)	7.38
	3DGS-MCMC	<b>22.45</b> (1)	<b>14.64</b> (1)	7.80
gazebo†	Official 3DGS	20.67 (3)	<b>12.50</b> (1)	8.17
	Mip-Splatting	21.29 (2)	11.89 (3)	9.40
	3DGS-MCMC	<b>22.60</b> (1)	12.36 (2)	10.24
yaris	Official 3DGS	17.74 (3)	10.56 (3)	7.18
	Mip-Splatting	18.58 (2)	10.82 (2)	7.75
	3DGS-MCMC	<b>18.62</b> (1)	<b>10.90</b> (1)	7.72
alps	Official 3DGS	17.34 (3)	14.08 (3)	3.27
	Mip-Splatting	17.96 (2)	14.31 (2)	3.65
	3DGS-MCMC	<b>19.04</b> (1)	<b>14.58</b> (1)	4.46
<b>Mean</b>	Official	22.21	14.26	<b>7.95</b>
	Mip-Splat	22.67	14.29	<b>8.38</b>
	MCMC	<b>23.37</b>	<b>14.50</b>	<b>8.87</b>

Two controls rule this out. (i) *Same-image control*: 31 images fall in *both* held-out sets (where the sector intersects every-8th positions). On these images—identical GT and viewpoint, only the training set differs—the gap is still +5.81 dB (all 31 positive), so it reflects model quality, not image difficulty (Appendix G). (ii) *Copy baseline*: copying the nearest training-view GT scores  $\sim 12$  dB for *both* arms (interp 12.6, extrap 11.7; a 0.9 dB difference), an order of magnitude smaller than the 3–11 dB model gap—so GT similarity to training views does not explain it (Appendix H).

## 5 Why Does the Gap Exist?

### 5.1 Angular Distance Drives the Gap

Figure 3 supports *angular distance to training views* as a major factor driving the gap. Across the 9 MipNeRF360 real-capture scenes (excluding truck because its Tanks-and-Temples camera geometry differs), extrap test views are  $4.1\times$  farther from their nearest training view than interp views (mean  $15.2^\circ$  vs.  $3.7^\circ$ ). This distance increase is expected—the sector holdout raises angular distance by

Table 3: **Fair matched-count interpolation–extrapolation gap.** Both arms train on  $N - K$  images; interp holds out every 8th (standard protocol), extrap holds out a contiguous sector (same  $K$ ). All eval images are genuinely unseen. \*Robust Mip-Splatting vs. Official reversal confirmed by multi-seed validation. Official 3DGS rows show mean $\pm$ std over 3 training seeds; Mip-Splatting and MCMC entries are single runs except for the additional Mip-Splatting seed runs used to validate starred reversals. IntR/ExtR = interpolation/extrapolation rank (1=best).

Scene	Method	Interp	Extrap	Gap	IntR	ExtR
bicycle*	Official 3DGS	25.12 $\pm$ .12	<b>18.89</b> $\pm$ .15	6.23 $\pm$ .03	3	1
	Mip-Splatting	<b>25.27</b>	18.63	6.64	1	2
	3DGS-MCMC	25.22	18.53	6.69	2	3
flowers	Official 3DGS	21.49 $\pm$ .07	18.15 $\pm$ .06	3.35 $\pm$ .02	2	2
	Mip-Splatting	21.36	18.10	3.27	3	3
	3DGS-MCMC	<b>21.52</b>	<b>18.35</b>	3.17	1	1
garden*	Official 3DGS	27.29 $\pm$ .05	<b>23.65</b> $\pm$ .09	3.63 $\pm$ .06	3	1
	Mip-Splatting	27.37	23.02	4.35	2	3
	3DGS-MCMC	<b>27.46</b>	23.57	3.89	1	2
stump	Official 3DGS	26.41 $\pm$ .24	<b>21.64</b> $\pm$ .50	4.77 $\pm$ .26	2	1
	Mip-Splatting	26.32	21.42	4.90	3	3
	3DGS-MCMC	<b>26.72</b>	21.59	5.13	1	2
treehill	Official 3DGS	22.38 $\pm$ .12	<b>16.36</b> $\pm$ .09	6.03 $\pm$ .04	2	1
	Mip-Splatting	21.94	16.14	5.80	3	3
	3DGS-MCMC	<b>22.40</b>	16.26	6.14	1	2
bonsai	Official 3DGS	32.07 $\pm$ .06	24.34 $\pm$ .23	7.74 $\pm$ .19	2	2
	Mip-Splatting	31.97	24.24	7.73	3	3
	3DGS-MCMC	<b>32.44</b>	<b>25.20</b>	7.24	1	1
counter	Official 3DGS	29.00 $\pm$ .07	17.91 $\pm$ .15	11.09 $\pm$ .22	3	3
	Mip-Splatting	29.15	18.19	10.95	2	2
	3DGS-MCMC	<b>29.18</b>	<b>18.31</b>	10.87	1	1
kitchen	Official 3DGS	31.18 $\pm$ .14	23.91 $\pm$ .12	7.26 $\pm$ .23	3	1
	Mip-Splatting	<b>31.45</b>	23.78	7.67	1	3
	3DGS-MCMC	<b>31.45</b>	23.79	7.66	2	2
room	Official 3DGS	31.39 $\pm$ .15	26.85 $\pm$ .24	4.54 $\pm$ .33	3	3
	Mip-Splatting	31.59	27.13	4.46	2	2
	3DGS-MCMC	<b>31.69</b>	<b>27.27</b>	4.42	1	1
truck	Official 3DGS	25.29 $\pm$ .08	21.48 $\pm$ .16	3.81 $\pm$ .10	2	2
	Mip-Splatting	25.26	21.28	3.98	3	3
	3DGS-MCMC	<b>26.03</b>	<b>22.08</b>	3.95	1	1
<b>Mean</b>	Official	27.16	21.32	<b>5.84</b>		
	Mip-Splat	27.17	21.19	<b>5.98</b>		
	MCMC	<b>27.41</b>	<b>21.50</b>	<b>5.92</b>		

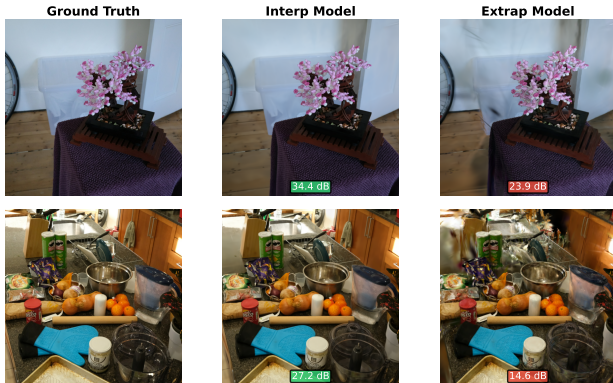


Figure 2: **Same-image comparison** (Official 3DGS, shared held-out images). Each row shows the *same ground-truth (GT) image* rendered by two models trained on different  $N-K$  images. The interp model (trained without every-8th frames) renders faithfully; the extrap model (trained without the azimuth sector containing this viewpoint) shows severe degradation, despite training on the same number of images. *This is not an image-difficulty effect*: on the 31 images held out by *both* arms the gap is still +5.81 dB, while copying the nearest training-view GT differs by only +0.9 dB between arms (§4).

*construction*—so the larger separation alone is not evidence that distance *causes* the gap. The mechanistic evidence is the per-image relationship: PSNR falls with nearest-view distance across all 492 held-out images (Pearson  $r = -0.58$ , Spearman  $\rho = -0.57$ ,  $p < 10^{-44}$ ), and, crucially, this trend holds *within* each scene individually (mean within-scene  $r = -0.66$ ,  $p < 0.005$  on all 9). The within-scene correlation removes the by-construction and scene-level confounds: quality degrades smoothly with distance even among held-out views of the same scene and arm. Simpler than learned uncertainty methods [53], nearest-view distance is not improved on by more complex features or nonlinear models in our data, making it an effective zero-cost diagnostic that flags interpolation-dominated evaluation without retraining (§7).

**Multi-sector robustness.** To verify that the gap is not an artifact of one particular holdout region, we rotate the sector start over 8 evenly-spaced azimuths on 4 scenes—2 outdoor (garden, bicycle) and 2 indoor (kitchen, bonsai)—for 32 additional runs. The gap is *positive at every sector position on every scene* (Table 4); magnitude varies (std 1.0–2.5 dB) but direction is invariant. The two indoor scenes—where an azimuth sector need not be spatially contiguous—show the same invariant gap, so the effect does not require a geometrically contiguous holdout. Main results use the seed-42 position.

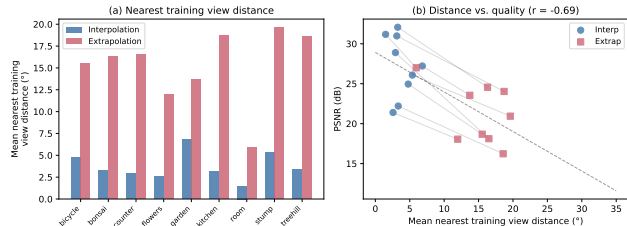


Figure 3: **Nearest training-view distance and the gap.** (a) By construction, extrapolation test views are  $4.1\times$  farther from their nearest training view than interpolation views (mean  $15.2^\circ$  vs.  $3.7^\circ$  across the 9 scenes). (b) The mechanistic test: per-image PSNR falls with nearest-view distance ( $n = 492$ ,  $r = -0.58$ ,  $p < 10^{-44}$ ), and the trend holds *within* every scene. Lines connect the two arms of each scene.

Table 4: **Multi-sector robustness** (8 sector positions per scene, Official 3DGS). The gap is positive at every position; magnitude varies with region difficulty.

Scene	Gap mean	Gap std	Min gap	Max gap
garden	+2.3	1.0	+0.8	+3.6
bicycle	+4.7	2.5	+1.4	+8.0
kitchen	+6.1	1.6	+3.7	+9.3
bonsai	+6.6	1.6	+3.7	+9.1

## 5.2 SH-Degree Decomposition of the Gap

To understand *why* the gap exists, we decompose it by spherical harmonic (SH) degree—a diagnostic any future paper can apply with zero retraining. SH coefficients above degree 0 encode view-dependent appearance; rendering at SH degree 0 produces a purely diffuse (view-independent) image. We render all extrap and interp test views at SH degrees 0–3 from the same trained model (Figure 4).

The gap at SH degree 0 (diffuse only) captures a *diffuse/geometry-proxy* component: with view-dependent color removed, the residual gap reflects Gaussians not positioned correctly for novel viewpoints. The additional gap from SH degrees 1–3 captures the *view-dependent* component: SH coefficients overfit to training-view directions. Across the same 9 MipNeRF360 scenes, **62%** of the gap is in the diffuse/geometry-proxy component and **38%** is view-dependent (Table 5). On 3 scenes (bicycle, stump, treehill), higher SH degrees actually *hurt* extrapolation PSNR—the model’s learned view-dependent colors are wrong for novel directions, consistent with SH overfitting to training views as documented by concurrent work on sparse-view settings [52]. *Caveat*: SH coefficients can compensate for geometric errors [24] (“appearance compensation”), so the geometric and view-dependent components interact rather than sum perfectly. The decomposition is approximate but

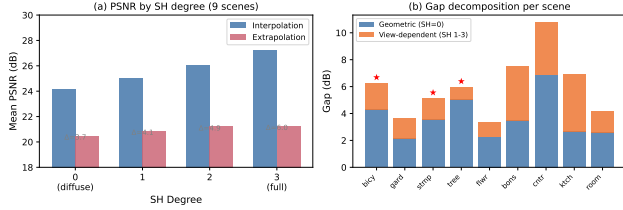


Figure 4: **Gap attribution by SH degree.** (a) Interp PSNR improves with SH degree (view-dependent color helps); extrap PSNR gains less. (b) Per-scene decomposition: blue = diffuse/geometry-proxy gap (SH=0), orange = view-dependent gap. Stars (\*) mark scenes where SH *hurts* extrapolation. Mean: 62% diffuse, 38% VD.

Table 5: **SH-degree decomposition of the gap** (seed-0 models). Gap@SH0 = gap using only diffuse color (a geometry-proxy component). VD contribution = Gap@SH3 – Gap@SH0. On 3 scenes (\*), higher SH *hurts* extrap PSNR. Diffuse/VD interact rather than sum exactly (see text).

Scene	Gap@SH0	Gap@SH3	Diff.%	VD%
bicycle*	+4.29	+6.27	68	32
garden	+2.17	+3.67	59	41
stump*	+3.55	+5.14	69	31
treehill*	+5.05	+5.98	84	16
flowers	+2.26	+3.34	68	32
bonsai	+3.47	+7.51	46	54
counter	+6.87	+10.78	64	36
kitchen	+2.67	+6.95	38	62
room	+2.60	+4.18	62	38
<b>Mean</b>			<b>62</b>	<b>38</b>

directionally informative.

### 5.3 The Gap Is Representation-Independent

The SH decomposition attributes most of the gap to the diffuse/geometry-proxy component rather than Gaussian-specific view-dependent color. If this reflects a genuine geometric cause, the gap should appear in a representation with *no* Gaussians and *no* SH at all. We test this directly with Instant-NGP, a volumetric NeRF that encodes the scene in a multi-resolution hash grid and a small MLP, rendered with nerfacc occupancy-grid sampling. We train it under the identical fair matched-count protocol—the same per-scene split files as Table 3, one model per arm, 20K steps—on the 9 MipNeRF360 scenes (Table 6).

The gap reproduces on **all 9 scenes** (mean **+3.73 dB**, 95% CI [2.14, 5.33]; sign test  $p = 0.002$ , paired  $t$ -test  $p = 6 \times 10^{-4}$ ). Crucially, the per-scene NeRF gap is strongly correlated with the 3DGS gap ( $r = 0.90$ ,  $p = 0.001$ ): counter is largest and flowers/stump smallest under both representa-

Table 6: **The gap in a non-Gaussian NeRF.** Instant-NGP (hash-grid + MLP, nerfacc volumetric rendering) under the same fair matched-count protocol as Table 3 (separate model per arm, identical splits, 20K steps), 9 MipNeRF360 scenes. All gaps positive; per-scene gap correlates with the 3DGS-Official gap at  $r = 0.90$ .

Scene	Interp	Extrap	Gap
garden	24.47	22.08	+2.39
bicycle	22.33	19.59	+2.74
flowers	20.01	18.51	+1.50
stump	20.80	19.32	+1.48
treehill	22.05	17.99	+4.06
bonsai	29.05	23.12	+5.93
counter	26.24	18.48	+7.76
kitchen	27.02	22.68	+4.34
room	29.70	26.29	+3.41
<b>Mean</b>	<b>24.63</b>	<b>20.90</b>	<b>+3.73</b>

tions, indicating a shared scene-geometric cause rather than a representation artifact. Interp PSNR matches published nerfacc NGP within  $\sim 1$ – $2$  dB (mean  $-1.65$  dB, i.e. slightly conservative), confirming the pipeline is faithful. The mean magnitude is smaller than 3DGS (5.8 dB), consistent with NeRF’s hash-grid interpolation degrading more gracefully off-distribution than explicit primitives—but the direction and per-scene structure are unmistakably the same.

### 5.4 Regularization

We also tested whether optimization-side interventions can close the gap: six training-time regularizers on all 10 real-capture scenes (Official 3DGS, extrap arm; Appendix K). The best (SH-degree annealing, view-dependent regularization) help only 9/10 scenes by  $+0.09$ – $0.17$  dB—modest against the 5.84 dB gap—while aggressive interventions destabilize training. The gap is largely a *data-coverage* problem, not one that loss-side tuning resolves.

## 6 Implications

Since loss-side tuning barely moves the gap, the practical lever is **capturing or generating more angularly diverse training views**, as the per-image distance correlation (Figure 3) predicts.

**Coverage-guided view selection.** If the gap is a data-coverage problem, strategically adding views should help more than random placement. We validate this on all 10 real-capture scenes: starting from the extrap training set, we add  $M \in \{1, 3, 5, 8\}$  images from the held-out sector, selected either by our coverage diagnostic (greedily picking views farthest from any training view) or randomly (5

Table 7: **Coverage-guided view selection** (10 scenes,  $M \in \{1, 3, 5, 8\}$  views added, 240 runs).  $\Delta$  = coverage – random mean (5 repeats). Bold = coverage above 95% CI of random ( $p < 0.05$ ).

Scene	$\Delta$ (coverage – random) dB			
	$M=1$	$M=3$	$M=5$	$M=8$
garden	<b>+0.88</b>	<b>+0.90</b>	+0.71	+0.93
bicycle	+0.27	+0.40	<b>+0.87</b>	+0.57
flowers	+0.33	+0.25	<b>+0.77</b>	<b>+0.55</b>
stump	+0.05	–0.98	–2.08	–0.64
treehill	–0.04	<b>+1.08</b>	+0.75	–0.32
bonsai	<b>+0.80</b>	–0.03	<b>+0.63</b>	<b>+1.17</b>
counter	<b>+1.66</b>	<b>+1.51</b>	+1.05	+0.66
kitchen	+0.95	+0.94	<b>+1.20</b>	<b>+0.97</b>
room	<b>+0.61</b>	<b>+0.62</b>	+0.18	–0.70
truck	<b>+0.54</b>	+0.22	–0.32	–0.81
<b>Win</b>	<b>9/10</b>	8/10	8/10	6/10
<b>Sig.</b>	5/10	4/10	4/10	3/10
$\Delta$	<b>+0.60</b>	+0.49	+0.38	+0.24

repeats per setting; 240 total runs). Coverage-guided selection outperforms random on **31/40** scene-budget combinations, with 16/40 significantly above the 95% CI of the random distribution ( $t$ -test,  $n = 5$ ; Table 7). The advantage is strongest at  $M = 1$ : adding a *single* well-placed view beats random on 9/10 scenes (+0.60 dB avg, 5/10 significant). *Note*: coverage adds gap-filling views to training, which also improves coverage of remaining eval images; both training improvement and eval-set coverage contribute to the observed gains. Unlike learned methods (FisherRF [54], COVER [55]) that require a trained model, our diagnostic needs only camera poses—applicable *before* any reconstruction begins (Appendix F).

**Downstream impact.** The gap also propagates to downstream perception proxies: across 6 scenes, depth estimated (Depth Anything V2 [51]) from extrap renders matches GT-photo depth worse on 5/6 scenes (root-mean-square error, RMSE, +42–248%) and no-reference perceptual quality (MUSIQ [50]) drops on 6/6 (mean –5.1%). These are proxy metrics (render-vs-GT-photo depth, no-reference quality), so we treat them as suggestive corroboration; full results are in Appendix J.

## 7 Discussion

**Implications for the field.** Standard near-trajectory holdouts are not wrong—they faithfully measure interpolation quality, which matters for many applications—but they should not, on their own, be read as evidence of spatial generalization. Because the gap exceeds the differences typically reported between published methods (Table 3), a

comparison claiming “0.5 dB better” can be smaller than the evaluation-mode effect; under multi-seed confirmation this is consequential enough to reverse two method rankings (garden, bicycle). We therefore recommend reporting a spatial-holdout metric *alongside* the standard one whenever generalization is claimed; the toolkit we are preparing for release reduces this to a one-line addition.

**Feed-forward generality.** We also evaluate two architecturally distinct feed-forward models that predict Gaussians from 2 input views—MVSplat [36] (cost-volume, ECCV’24) and DepthSplat [37] (DPT + Depth Anything, CVPR’25)—with context views sampled from images available to both arms (mean±std over 3 seeds; Appendix I). Zero-shot on the 9 MipNeRF360 scenes ( $256 \times 256$ ), the gap is positive in **46/54** method-scene-seed combinations (sign test  $p < 10^{-5}$ ; MVSplat  $+0.99 \pm 1.00$  dB, DepthSplat  $+1.56 \pm 1.16$  dB), though absolute PSNR is low ( $\sim 8$ – $10$  dB) due to domain mismatch. Evaluating *in-domain* on 38 RealEstate10K test scenes with each method’s official pipeline (identical preprocessing; only the target frames change, from published-nearby to farthest-from-context) removes that confound: DepthSplat **+7.3 dB** (25.5/18.3), MVSplat **+9.1 dB** (25.7/16.6). This feed-forward test uses a *distance-based target* protocol (nearby vs. farthest-from-context), an analogous stress test of the interpolation-vs-extrapolation axis rather than our exact azimuth-sector split. Across optimization-based Gaussians and a volumetric NeRF (matched-count sector, §5.3) and feed-forward Gaussians (distance-based target), the gap appears in all three representation families—evidence it is tied to spatial coverage, not to any single representation or to per-scene overfitting.

**Limitations.** The sector holdout is one specific structured holdout; however, the per-image correlation ( $r = -0.58$ ) predicts that *any* holdout increasing angular distance would produce a similar gap. The azimuth-based sector may not map to a contiguous spatial region for indoor scenes. Our cross-representation evaluation covers two feed-forward methods and one volumetric NeRF (Instant-NGP) on nine scenes; broader coverage across additional feed-forward and NeRF architectures is left to future work. Some ranking changes are seed-sensitive; we treat only garden and bicycle as robust reversals. The capture planning experiment selects from existing held-out images rather than generating truly new viewpoints.

**Training non-determinism.** 3DGS training is non-deterministic (atomicAdd in the backward pass). Across 3 seeds on all 10 scenes (Official 3DGS), the mean gap is  $39 \times$  the mean seed std (worst case room,  $13 \times$ ), and the di-

rection is positive on all 30 scene-seed combinations (Appendix B).

**Recommended evaluation practice.** We recommend future 3DGS papers report: (1) standard `test_every=N` for comparability; (2) a spatial-holdout metric (one extra training run); (3) the holdout construction rule; and (4) nearest-training-view angular distance per test view—a zero-cost diagnostic that flags interpolation-dominated evaluation even without retraining.

**Reproducibility.** The supplement documents every split-construction rule, per-scene configuration, and baseline commit hash, and an artifact manifest (Appendix D) maps every table and figure to its generating procedure and source data; code is in preparation for release (§1).

## 8 Conclusion

Standard MipNeRF360-style 3DGS evaluation primarily measures near-trajectory interpolation. Our fair matched-count protocol isolates a consistent **3–12 dB** gap—larger than inter-method differences, robust to training noise, and reproduced across three representation families including a non-Gaussian NeRF. It should be reported via a spatial-holdout metric *alongside* the standard one when generalization is claimed; our toolkit makes this practical.

## References

- [1] B. Kerbl, G. Kopanas, T. Leimkühler, and G. Drettakis. 3D Gaussian Splatting for real-time radiance field rendering. *ACM Trans. Graph.*, 42(4), 2023.
- [2] HunyuanWorld Team. HY-World 2.0: A multi-modal world model for reconstructing, generating, and simulating 3D worlds. *arXiv preprint arXiv:2604.14268*, 2026.
- [3] H.-X. Yu, H. Duan, C. Herrmann, W. T. Freeman, and J. Wu. WonderWorld: Interactive 3D scene generation from a single image. In *CVPR*, 2025.
- [4] R. Gao, *et al.* CAT3D: Create anything in 3D with multi-view diffusion models. In *NeurIPS*, 2024.
- [5] W. Yu, *et al.* ViewCrafter: Taming video diffusion models for high-fidelity novel view synthesis. *IEEE TPAMI*, 2025.
- [6] J. T. Barron, B. Mildenhall, D. Verbin, P. P. Srinivasan, and P. Hedman. Mip-NeRF 360: Unbounded anti-aliased neural radiance fields. In *CVPR*, 2022.
- [7] A. Knapitsch, J. Park, Q.-Y. Zhou, and V. Koltun. Tanks and Temples: Benchmarking large-scale scene reconstruction. *ACM Trans. Graph.*, 36(4), 2017.
- [8] R. Martin-Brualla, N. Radwan, M. S. M. Sajjadi, *et al.* NeRF in the Wild: Neural radiance fields for unconstrained photo collections. In *CVPR*, 2021.
- [9] Y. Ye, R. Li, J. Kerr, M. Turkulainen, *et al.* gsplat: An open-source library for Gaussian Splatting. *JMLR*, 26(34), 2025.
- [10] J. Kulhanek and T. Sattler. NerfBaselines: Consistent and reproducible evaluation of novel view synthesis methods. In *NeurIPS Datasets & Benchmarks*, 2025.
- [11] Z. Ye, *et al.* AbsGS: Recovering fine details for 3D Gaussian Splatting. In *ACM MM*, 2024.
- [12] Z. Yu, *et al.* Mip-Splatting: Alias-free 3D Gaussian Splatting. In *CVPR*, 2024.
- [13] J. C. Lee, D. Rho, X. Sun, J. H. Ko, and E. Park. Compact 3D Gaussian representation for radiance field. In *CVPR*, 2024.
- [14] B. Huang, Z. Yu, A. Chen, A. Geiger, and S. Gao. 2D Gaussian Splatting for geometrically accurate radiance fields. In *SIGGRAPH*, 2024.
- [15] Y. Liang, X. Yang, J. Lin, H. Li, X. Xu, and Y. Chen. LucidDreamer: Towards high-fidelity text-to-3D generation via interval score matching. In *CVPR*, 2024.
- [16] K. Sargent, Z. Li, T. Shah, C. Herrmann, H.-X. Yu, Y. Zhang, *et al.* ZeroNVS: Zero-shot 360-degree view synthesis from a single image. In *CVPR*, 2024.
- [17] B. Mildenhall, P. P. Srinivasan, M. Tancik, J. T. Barron, R. Ramamoorthi, and R. Ng. NeRF: Representing scenes as neural radiance fields for view synthesis. In *ECCV*, 2020.
- [18] F. Warburg, E. Weber, M. Tancik, A. Holynski, and A. Kanazawa. Nerfbusters: Removing ghostly artifacts from casually captured NeRFs. In *ICCV*, 2023.
- [19] X. Chen, Q. Zhang, X. Li, Y. Chen, Y. Feng, X. Wang, and J. Wang. Hallucinated neural radiance fields in the wild. In *CVPR*, 2022.
- [20] D. Kotovenko, O. Grebenkova, and B. Ommer. EDGS: Eliminating densification for efficient convergence of 3DGS. In *CVPR*, 2026.
- [21] X. Han, *et al.* Extrapolated urban view synthesis benchmark. In *ICCV*, 2025.
- [22] S. Hwang, M.-J. Kim, T. Kang, J. Kang, and J. Choo. VEGS: View Extrapolation of Urban Scenes in 3D Gaussian Splatting using Learned Priors. In *ECCV*, 2024.
- [23] S. Cerezo, G. Meli, T. Berriel Martins, K. Safronov, and J. Civera. SLAM&Render: A benchmark for the intersection of neural rendering and SLAM. *arXiv preprint arXiv:2504.13713*, 2025.
- [24] K. Xiong, *et al.* ICO-GS: Intrinsic geometry-appearance consistency optimization for sparse-view Gaussian Splatting. *arXiv preprint arXiv:2603.02893*, 2026.
- [25] X. Xu, *et al.* DropoutGS: Dropping out Gaussians for better sparse-view rendering. In *CVPR*, 2025.
- [26] Y. Xing, *et al.* 3DGS-IEval-15K: A large-scale image quality evaluation database for 3D Gaussian Splatting. In *ACM MM*, 2025.
- [27] Y. Lan, *et al.* Geo-EVS: Geometry-conditioned extrapolative view synthesis for autonomous driving. *arXiv preprint arXiv:2604.07250*, 2026.
- [28] K. Tan, *et al.* ExtraGS: Geometric-aware trajectory extrapolation with uncertainty-guided generative priors. *arXiv preprint arXiv:2508.15529*, 2025.

- [29] A. Paliwal, *et al.* CoherentGS: Sparse novel view synthesis with coherent 3D Gaussians. In *ECCV*, 2024.
- [30] S. Kheradmand, D. Rebain, G. S. Sharma, W. Sun, Y. C. Tseng, H. Isack, A. Kar, A. Tagliasacchi, and K. M. Yi. 3D Gaussian Splatting as Markov chain Monte Carlo. In *NeurIPS*, 2024.
- [31] T. Lu, M. Yu, L. Xu, Y. Xiangli, L. Wang, D. Lin, and B. Dai. Scaffold-GS: Structured 3D Gaussians for view-adaptive rendering. In *CVPR*, 2024.
- [32] G. Fang, *et al.* Mini-Splatting: Representing scenes with a constrained number of Gaussians. In *ECCV*, 2024.
- [33] K. Cheng, *et al.* GaussianPro: 3D Gaussian Splatting with progressive propagation. In *ICML*, 2024.
- [34] Y. Wang, *et al.* FreeSplat: Generalizable 3D Gaussian Splatting towards free-view synthesis of indoor scenes. In *NeurIPS*, 2024.
- [35] D. Charatan, S. Li, A. Tagliasacchi, and V. Sitzmann. pixelSplat: 3D Gaussian Splats from image pairs for scalable generalizable 3D reconstruction. In *CVPR*, 2024.
- [36] Y. Chen, H. Xu, C. Zheng, B. Zhuang, M. Pollefeys, A. Geiger, T. H. Cai, and J. Liang. MVSPat: Efficient 3D Gaussian Splatting from sparse multi-view images. In *ECCV*, 2024.
- [37] H. Xu, B. Peng, Z. Cai, H. Zhou, B. Zhuang, and S. Soatto. DepthSplat: Connecting Gaussian Splatting and Depth. In *CVPR*, 2025.
- [38] Z. Fan, *et al.* InstantSplat: Unbounded sparse-view pose-free Gaussian Splatting in 40 seconds. *arXiv preprint arXiv:2403.20309*, 2024.
- [39] M. Turkulainen, *et al.* DN-Splatter: Depth and normal priors for Gaussian Splatting and meshing. In *WACV*, 2025.
- [40] A. Hanson, A. Tu, V. Singla, M. Jayawardhana, M. Zwicker, and T. Goldstein. PUP 3D-GS: Principled uncertainty pruning for 3D Gaussian Splatting. In *CVPR*, 2025.
- [41] J. Kulhanek, S. Peng, Z. Kukulova, M. Pollefeys, and T. Sattler. WildGaussians: 3D Gaussian Splatting in the wild. In *NeurIPS*, 2024.
- [42] Q. Wang, L. Fan, Y. Wang, Y. Chen, and Z. Zhang. FreeVS: Generative view synthesis on free driving trajectory. In *ICLR*, 2025.
- [43] W. Xiao, R. Santa Cruz, D. Ahmedt-Aristizabal, O. Salvado, C. Fookes, and L. Lebrat. NeRF Director: Revisiting view selection in neural volume rendering. In *CVPR*, 2024.
- [44] K. Liu, *et al.* ViewExtrapolator: Novel view extrapolation with video diffusion priors. *arXiv preprint arXiv:2411.14208*, 2024.
- [45] M. Shih, W. Ma, *et al.* ExtraNeRF: Visibility-aware view extrapolation of neural radiance fields with diffusion models. In *CVPR*, 2024.
- [46] M. Niemeyer, J. T. Barron, B. Mildenhall, M. S. M. Sajjadi, A. Geiger, and N. Radwan. RegNeRF: Regularizing neural radiance fields for view synthesis from sparse inputs. In *CVPR*, 2022.
- [47] H. Park, G. Ryu, and W. Kim. DropGaussian: Structural regularization for sparse-view Gaussian Splatting. In *CVPR*, 2025.
- [48] Y. Yun, *et al.* FASR: Frequency-adaptive sharpness regularization for improving 3D Gaussian Splatting generalization. *arXiv preprint arXiv:2511.17918*, 2025.
- [49] K. Chen, Y. Zhong, Z. Li, J. Lin, Y. Chen, M. Qin, and H. Wang. Quantifying and alleviating co-adaptation in sparse-view 3D Gaussian Splatting. In *NeurIPS*, 2025.
- [50] J. Ke, Q. Wang, Y. Wang, P. Milanfar, and F. Yang. MUSIQ: Multi-scale image quality transformer. In *ICCV*, 2021.
- [51] L. Yang, B. Kang, Z. Huang, Z. Zhao, X. Xu, J. Feng, and H. Zhao. Depth Anything V2. In *NeurIPS*, 2024.
- [52] G. Fang, *et al.* Dropping Anchor and Spherical Harmonics for Sparse-view Gaussian Splatting. In *CVPR*, 2026.
- [53] T. Gottwald, *et al.* PRIMU: Uncertainty estimation for novel views in Gaussian Splatting from primitive-based representations of error and coverage. *arXiv preprint arXiv:2508.02443*, 2025.
- [54] J. Jiang, *et al.* FisherRF: Active view selection and uncertainty quantification for radiance fields using Fisher information. In *ECCV*, 2024.
- [55] J. Chen, *et al.* COVER: Coverage optimization for camera view selection. In *CVPR*, 2026.
- [56] T. Müller, A. Evans, C. Schied, and A. Keller. Instant neural graphics primitives with a multiresolution hash encoding. *ACM Trans. Graph.*, 41(4):102:1–102:15, 2022.
- [57] R. Li, M. Tancik, and A. Kanazawa. NerfAcc: A general NeRF acceleration toolbox. *arXiv preprint arXiv:2210.04847*, 2022.

## Appendix: Supplementary Material

This appendix provides multi-metric results, multi-seed validation details, method configurations, and an artifact manifest. All results use the **fair matched-count protocol** (both arms train on  $N - K$  images, evaluate on  $K$  genuinely unseen images).

### A Multi-Metric Results (SSIM and LPIPS)

Table 8 reports the SSIM and LPIPS gap alongside PSNR for real-capture scenes (Official 3DGS, seed 0). The gap is consistent across all three metrics on every scene.

Table 8: Multi-metric gap on 10 real-capture scenes (Official 3DGS, fair matched-count protocol, single seed).  $\Delta$ PSNR/SSIM = interp - extrap (positive = interp better). LPIPS is shown raw (lower = better).

Scene	PSNR (dB)			SSIM		LPIPS	
	Int	Ext	$\Delta$	Int	Ext	Int	Ext
bicycle	24.96	18.68	+6.27	.754	.551	.216	.334
bonsai	32.07	24.56	+7.51	.941	.883	.207	.323
counter	28.90	18.12	+10.78	.907	.708	.203	.347
flowers	21.40	18.06	+3.34	.595	.486	.341	.388
garden	27.22	23.55	+3.67	.863	.779	.109	.170
kitchen	30.98	24.03	+6.95	.925	.821	.130	.214
room	31.18	27.00	+4.18	.917	.872	.224	.257
stump	26.08	20.94	+5.14	.751	.550	.227	.348
treehill	22.21	16.23	+5.98	.624	.464	.329	.398
truck	25.17	21.31	+3.87	.878	.806	.150	.221
<b>Mean</b>	27.02	21.25	<b>+5.77</b>	.815	.692	.214	.300

### B Multi-Seed Validation

The main real-capture table reports Official 3DGS results as mean $\pm$ std over 3 training seeds (seeds 0, 1, 2) on all 10 real-capture scenes. Each scene-method pair trains *two separate models* (one per arm), so training noise is independent between arms—it does *not* cancel. Nevertheless, the gap is robust:

- The gap is positive on all 30 scene-seed combinations.
- Seed-to-seed gap std ranges from 0.02 dB (flowers) to 0.33 dB (room), while the gap itself ranges from 3.4 to 11.1 dB.
- The mean gap (5.84 dB) is 39 $\times$  larger than the mean seed std (0.15 dB).
- Even the worst-case scene (room: 4.54 $\pm$ 0.33 dB) has a gap/noise ratio of 13.6 $\times$ .

Mip-Splatting has multi-seed validation (2–5 seeds) on the two reversal scenes (garden, bicycle); other Mip and all

MCMC rows are single runs. The consistent gap direction across all 48 scene-method combinations (16 scenes  $\times$  3 methods, including the single-run methods) provides additional breadth-based robustness, although the scene-method combinations are not statistically independent.

### C Method Configurations

Optimization-based methods trained with 30K iterations on the same data splits. Total: 502 optimization-based training runs (96 main + 40 Official multi-seed + 40 Mip multi-seed + 32 multi-sector + 54 regularizers + 240 capture planning) plus 130 feed-forward inference evaluations (54 cross-domain on MipNeRF360 + 76 in-domain on RealEstate10K).

Table 9: Training configurations for cross-method comparison.

Parameter	Official 3DGS	Mip-Splatting
Iterations	30,000	30,000
SH degree	3	3
Resolution	default (-1)	default (-1)
Densification	standard	standard
kernel_size	—	0.1
Seeds	0, 1, 2	0 (main); 1–2+ for reversals
3DGS-MCMC		
cap_max	scene-dependent (1.3–5.9M)	
noise_lr	5e5	
scale_reg	0.01	
opacity_reg	0.01	
init_type	sfm	
seed	42	

### D Artifact Manifest

Every number in the main text traces to tracked result summaries or per-run JSON files. Real-capture split JSONs are stored alongside their per-scene result folders. The public benchmark summary is `lto_benchmark/baselines.json`; the training-command manifest is stored under `results/fair_lto/`. In the manifest below, `R` abbreviates `results/fair_lto`.

- **Generated-view table:** the benchmark summary stores the released generated-scene baseline results; per-run outputs use `method/split` subdirectories when the generated result bundle is present.
- **Real-capture table:** per-scene folders contain Official 3DGS, Mip-Splatting, and MCMC `method/split` subdirectories with `lto_eval.json` summaries.
- **Multi-sector table:** `R/multi_sector/{scene}/sector*/eval.json`.

- **SH-decomposition** **table:** `R/sh.decomposition/{scene}.json`.
- **Regularizer table:** `R/{scene}/reg_{name}_extrap/lto_eval.json`. Launcher commands are generated by `scripts/launch_all_tracks.sh` and `scripts/run_exp_round2.sh`.
- **Downstream table:** `R/downstream_depth/{scene}/depth_results.json`; `R/downstream_impact/{scene}/results.json`.
- **Same-image control:** `R/same_image_control/summary.json`, with per-image inputs sourced from `R/sh.decomposition/{scene}.json`.
- **Feed-forward (MVSplat + DepthSplat):** `R/{scene}/mvsplat_seed{42,123,7}.json` and `R/{scene}/depthsplat_seed{42,123,7}.json` (9 scenes  $\times$  3 seeds  $\times$  2 methods = 54 files). Inference scripts: `scripts/eval_mvsplat_feedforward.py`, `scripts/eval_depthsplat_feedforward.py`. Sources (git submodules): `third_party/mvsplat/`, `third_party/depthsplat/`.
- **NGP NeRF table:** `R/{scene}/nerf_ngp_{interp,extrap}.json` (9 scenes  $\times$  2 arms = 18 files). Training script: `scripts/train_ngp_nerf_lto.py`; build and patch notes in `third_party/README.md`.
- **Nearest-image copy baseline:** `R/nearest_image_baseline/summary.json` (per-scene PSNR and SSIM for both splits).
- **Capture-planning table:** `R/capture_planning/` (coverage vs. random,  $M \in \{1, 3, 5, 8\}$ , 5 repeats, 240 runs).
- **Feed-forward in-domain (RealEstate10K):** `R/re10k_indomain/{mvsplat,depthsplat}_re10k.json` and the modified target index `evaluation_index_re10k_extrap.json`.
- **Figures:** generated by `scripts/generate_figures.py` (quantitative panels) and `scripts/render_qualitative.py` (same-image qualitative comparison), reading the result JSONs above.

The released toolkit scripts are under `lto_benchmark/`; the larger experiment launchers under `scripts/` use the repo-relative path configuration in `scripts/env.sh`. The released bundle uses repo-relative paths throughout; absolute machine paths are scrubbed before packaging.

**Baseline commit hashes.** For exact reproducibility, baselines were run at fixed upstream commits: Official 3DGS `b9da16c`, Mip-Splatting `dda02ab`, 3DGS-MCMC `7b4fc9f`; NGP NeRF uses `nerfacc` with Instant-NGP hash encoding (`tiny-cuda-nn`), with build details in `third_party/README.md`.

## E Spatial-Holdout Benchmark Toolkit

We release a *spatial-holdout benchmark toolkit* with standardized splits, evaluation scripts, and baseline results. The repository keeps the historical `lto_benchmark/` directory name for compatibility with the launch scripts. Usage:

```
# 1. Create sector holdout split
python lto_benchmark/create_sector_holdout.py \
  --source_path /path/to/colmap_scene \
  --output split_extrap.json

# 2. Train with held-out sector removed
python train.py -s data_ext -m model_ext \
  --iterations 30000

# 3. Evaluate on held-out views
python lto_benchmark/evaluate_lto.py \
  --source_path /path/to/full_scene \
  --model_path model_ext \
  --split split_extrap.json

# 4. Coverage diagnostic
python lto_benchmark/coverage_diagnostic.py \
  --source_path /path/to/colmap_scene
```

Output: `lto_eval.json` with PSNR, SSIM, LPIPS per image. The coverage diagnostic reports mean nearest-neighbor distance, largest angular gap, and recommended view positions—a zero-cost check for interpolation-dominated evaluation.

Contents: `lto_benchmark/` contains `create_sector_holdout.py`, `evaluate_lto.py`, `coverage_diagnostic.py`, and `baselines.json` (16 scenes  $\times$  3 methods).

## F View Selection Method Comparison

Table 10 compares our coverage-guided view selection against existing learned approaches. Our method’s key advantage is *pre-training applicability*: it uses only camera poses (available from COLMAP before any 3DGS training), enabling capture planning at the data-collection stage rather than the reconstruction stage. This is important for practical workflows where a practitioner must decide where to place cameras *before* investing in expensive 3DGS/NeRF training.

Table 10: Comparison of view selection methods. Our coverage diagnostic is the only zero-cost, pre-training-applicable approach.

Method	Trained model?	GPU cost	Pre-train applicable?	Quality signal
FisherRF [54]	Yes	High	No	Fisher info
COVER [55]	Yes	Medium	No	Projection
PRIMU [53]	Yes	Medium	No	Learned feat.
<b>Ours</b>	<b>No</b>	<b>Zero</b>	<b>Yes</b>	Angular dist.

The practical importance: in robotics path planning, real-estate scanning, autonomous driving data collection, and

world-model training pipelines, the camera placement decision must be made *before* any 3D reconstruction. Learned methods cannot help at this stage because they require an already-trained model. Our coverage diagnostic fills this gap by providing actionable guidance from camera poses alone, validated by the capture planning experiment (Table 7) where coverage-guided selection outperforms random on 31/40 scene-budget combinations (10 scenes, 240 runs).

## G Same-Image Control

A potential confound is that the interp and extrap arms evaluate mostly different images. To rule out image-difficulty effects, we identify images appearing in *both* eval sets (2–5 per scene, 31 total across 9 MipNeRF360 scenes). On these shared images, both the interp model and the extrap model are evaluated against the *same GT image*—the only difference is which model rendered it. The gap on shared images is +5.81 dB (comparable to the overall mean gap of 5.84 dB), with all 31 positive (Table 11).

Table 11: Same-image control: gap on images in both eval sets.

Scene	Shared	Mean gap (dB)	All pos?
garden	3	+3.92	Yes
bicycle	2	+1.84	Yes
flowers	4	+2.12	Yes
stump	2	+2.90	Yes
treehill	3	+2.97	Yes
bonsai	5	+8.35	Yes
counter	4	+9.40	Yes
kitchen	4	+8.19	Yes
room	4	+7.35	Yes
<b>Total</b>	<b>31</b>	<b>+5.81</b>	<b>Yes</b>

Result JSON: `summary.json` under `R/same_image_control/`. Per-image data comes from `{scene}.json` under `R/sh_decomposition/`.

## H Nearest-Image Copy Baseline

Table 12 reports per-scene PSNR and SSIM for the nearest-training-GT copy baseline. For each held-out image, we find the nearest training image by angular distance and compute metrics between the two GT photographs. The small copy gap (0.9 dB PSNR, 0.013 SSIM) compared to the model gap (3–11 dB) confirms that the model gap is not explained by GT image similarity alone.

## I Feed-Forward Generality: Per-Scene Results

Tables 13 and 14 report per-scene results for two architecturally distinct feed-forward models. For each scene, 2 con-

Table 12: Nearest-image copy baseline: PSNR and SSIM between each held-out GT and its nearest training GT. The copy gap is several-fold to an order of magnitude smaller than the model gap.

Scene	Copy PSNR (dB)			Copy SSIM		
	Int	Ext	$\Delta$	Int	Ext	$\Delta$
garden	14.6	13.8	+0.8	.144	.144	.000
bicycle	11.3	11.8	-0.5	.112	.124	-.012
flowers	9.0	9.5	-0.5	.082	.096	-.014
stump	13.2	12.7	+0.5	.146	.125	+0.021
treehill	9.3	11.0	-1.7	.124	.128	-.004
bonsai	15.1	13.6	+1.5	.445	.538	-.093
counter	13.6	10.2	+3.4	.391	.274	+0.117
kitchen	15.2	12.4	+2.8	.296	.249	+0.047
room	12.1	10.5	+1.6	.405	.354	+0.051
<b>Mean</b>	<b>12.6</b>	<b>11.7</b>	<b>+0.9</b>	<b>.238</b>	<b>.226</b>	<b>+0.013</b>

text views are selected from images available to both interp and extrap arms via farthest-point sampling; 3 context-selection seeds vary the initialization. All evaluations use  $256 \times 256$  with aspect-ratio-preserving rescale and center crop, matching each model’s training pipeline.

**MVSplat** [36] (ECCV’24 Oral) uses a cost-volume encoder with a UniMatch backbone; we use `re10k.ckpt`. **DepthSplat** [37] (CVPR’25) uses a DPT head with a Depth Anything V2 / DINOv2 backbone; we use the base  $256 \times 256$  2-view checkpoint. The `xformers` dependency was replaced with PyTorch’s native `scaled_dot_product_attention` for hardware portability (verified to produce identical PSNR).

Table 13: MVSplat feed-forward evaluation. Gap = interp – extrap PSNR (dB).

Scene	Seed 42	Seed 123	Seed 7	Mean±Std	3/3?
garden	+1.00	-0.01	-0.45	+0.18±0.61	
bicycle	+1.67	+1.00	+1.43	+1.37±0.28	✓
flowers	-0.14	+0.51	+0.76	+0.38±0.38	
stump	+2.35	+2.45	+2.57	+2.46±0.09	✓
treehill	+0.40	+0.92	+1.00	+0.77±0.27	✓
bonsai	+2.40	+2.93	+2.34	+2.56±0.27	✓
counter	+0.99	+1.07	+0.98	+1.01±0.04	✓
kitchen	-0.99	-0.48	+0.16	-0.44±0.47	
room	+0.97	+0.47	+0.46	+0.63±0.24	✓
<b>Overall:</b>	22/27 positive ( $p < 0.002$ )			<b>+0.99±1.00</b>	6/9

## J Downstream Impact

We test whether the gap propagates to downstream perception proxies on 6 MipNeRF360 scenes where depth and per-

Table 14: DepthSplat feed-forward evaluation. Gap = interp – extrap PSNR (dB).

Scene	Seed 42	Seed 123	Seed 7	Mean±Std	3/3?
garden	+1.24	+2.11	+1.17	+1.51±0.43	✓
bicycle	+0.73	+2.64	+1.96	+1.78±0.79	✓
flowers	+0.55	-0.12	+1.36	+0.60±0.61	
stump	+2.73	+0.50	+2.71	+1.98±1.05	✓
treehill	+1.33	+1.41	+2.84	+1.86±0.69	✓
bonsai	+3.92	+3.74	+3.70	+3.79±0.10	✓
counter	+1.74	+1.44	+1.54	+1.57±0.12	✓
kitchen	+1.24	+1.14	+0.82	+1.07±0.18	✓
room	-0.17	+0.27	-0.45	-0.12±0.30	
<b>Overall:</b>	24/27 positive ( $p < 0.0001$ )			<b>+1.56±1.16</b>	7/9

ceptual proxies were available (Official 3DGS, fair protocol; Table 15).

*Depth estimation.* We run Depth Anything V2 [51] on rendered images and measure how well the estimated depth matches depth estimated from the corresponding GT photograph (Pearson correlation and RMSE). On **5/6 scenes**, extrap renders produce less consistent depth (RMSE +42–248%). This is a proxy for geometric fidelity (comparing depth from renders vs. from GT photos, not metric depth).

*Perceptual quality.* No-reference perceptual quality (MUSIQ [50]) drops on all 6/6 scenes (mean -5.1%), suggesting perceptual degradation consistent with the PSNR gap. Both are proxy-on-proxy measurements and should be read as suggestive rather than definitive.

Table 15: **Downstream impact** on 6 real scenes (Official 3DGS). Depth: RMSE between depth(render) and depth(GT photo); lower = better. MUSIQ: no-reference perceptual quality; higher = better. †Room is the only scene where extrap depth RMSE improves.

Scene	Depth RMSE (↓)			MUSIQ (↑)	
	Interp	Extrap	Δ%	Interp	Extrap
bicycle	.022	.042	+92	73.8	69.4
bonsai	.024	.040	+69	62.5	61.4
counter	.021	.074	+248	61.1	58.5
garden	.012	.018	+42	75.7	74.2
kitchen	.014	.025	+75	68.6	62.7
room†	.049	.035	-28	55.0	50.6
<b>Mean</b>	<b>.024</b>	<b>.039</b>	<b>+83</b>	<b>66.1</b>	<b>62.8</b>

## K Regularization Ablation

To test whether optimization-side interventions can improve spatial-holdout quality, we evaluate six training-time regularizers on all 10 real-capture scenes (Official 3DGS, ex-

trap arm, 30K steps; Table 16). **SH degree annealing** (delaying SH degree increases to 7.5K/15K/22.5K) improves **9/10** scenes (+0.17 dB mean). **View-dependent regularization** (penalizing color variation under small camera perturbations) also improves 9/10. **Scale regularization** improves 8/10. All three outperform Gaussian dropout [25, 47] (2/10, -0.39 dB) and camera jitter (2/10, -2.85 dB). Coverage-Aware Training (CAT), a purpose-designed aggressive intervention, worsens all 9 tested scenes (-3.1 dB), demonstrating that aggressive regularization destabilizes training. The mild regularizers’ improvements (+0.09–0.17 dB) are modest compared to the gap itself (5.84 dB), reinforcing that the gap is largely a data-coverage problem.

Table 16: **Regularizer comparison on extrapolation PSNR** (10 scenes, Official 3DGS, 30K steps). ↑ = scenes improved vs. multi-seed baseline. SH annealing and view-dependent regularization each improve 9/10 scenes.

Method	Mean Δ (dB)	↑	Note
Dropout 30%	-0.39	2/10	Hurts most scenes
Cam jitter 2°	-2.85	2/10	Too aggressive
SH anneal	<b>+0.17</b>	<b>9/10</b>	Best mean gain
ViewDep reg	+0.12	<b>9/10</b>	Consistent
Scale reg	+0.09	8/10	Consistent
CAT†	-3.10	0/9	Destabilizes

†Coverage-Aware Training (SH reset + virtual camera 10° + opacity entropy); tested on 9 scenes.

## L Protocol Audit of Recent 3DGS Papers

Table 17 surveys 11 recent 3DGS papers. The split protocol for each entry was verified from the paper’s released source code (training scripts or config files) or, where code was unavailable, from the paper’s methodology section describing the evaluation split. All use `l1ffhold=8` (every 8th image as test) on smooth-trajectory datasets, making all vulnerable to the interpolation-extrapolation gap documented in the main text.

Table 17: Evaluation protocol audit. All 11 papers use the same near-trajectory holdout on smooth captures. Provenance: how the split protocol was verified.

Paper	Venue	Dataset	Split	Provenance
3DGS [1]	TOG’23	MipNeRF360	every 8th	code
Mip-Splatting [12]	CVPR’24	MipNeRF360	every 8th	code
3DGS-MCMC [30]	NeurIPS’24	MipNeRF360	every 8th	code
2DGS [14]	SIGGRAPH’24	MipNeRF360	every 8th	code
Scaffold-GS [31]	CVPR’24	MipNeRF360	every 8th	code
Compact3D [13]	CVPR’24	MipNeRF360	every 8th	code
AbsGS [11]	ACMMM’24	MipNeRF360	every 8th	code
DropGaussian [47]	CVPR’25	MipNeRF360	every 8th	code
DropoutGS [25]	CVPR’25	MipNeRF360	every 8th	code
EDGS [20]	CVPR’26	MipNeRF360	every 8th	code
DropAnSH [52]	CVPR’26	MipNeRF360	every 8th	paper